Observations of Precipitation Size and Fall Speed Characteristics within Coexisting Rain and Wet Snow

SANDRA E. YUTER
Department of Marine, Earth, and Atmospheric Sciences, North Carolina State University, Raleigh, North Carolina

DAVID E. KINGSMILL
Cooperative Institute for Research in Environmental Sciences, University of Colorado, Boulder, Colorado

LOUISA B. NANCE
National Center for Atmospheric Research, Boulder, Colorado*

MARTIN LÖFFLER-MANG
University of Applied Sciences, Saarbrücken, Germany

(Manuscript received 13 May 2005, in final form 31 January 2006)

ABSTRACT

Ground-based measurements of particle size and fall speed distributions using a Particle Size and Velocity (PARSIVEL) disdrometer are compared among samples obtained in mixed precipitation (rain and wet snow) and rain in the Oregon Cascade Mountains and in dry snow in the Rocky Mountains of Colorado. Coexisting rain and snow particles are distinguished using a classification method based on their size and fall speed properties. The bimodal distribution of the particles' joint fall speed–size characteristics at air temperatures from 0.5° to 0°C suggests that wet-snow particles quickly make a transition to rain once melting has progressed sufficiently. As air temperatures increase to 1.5°C, the reduction in the number of very large aggregates with a diameter > 10 mm coincides with the appearance of rain particles larger than 6 mm. In this setting, very large raindrops appear to be the result of aggregrates melting with minimal breakup rather than formation by coalescence. In contrast to dry snow and rain, the fall speed for wet snow has a much weaker correlation between increasing size and increasing fall speed. Wet snow has a larger standard deviation of fall speed (120%–230% relative to dry snow) for a given particle size. The average fall speed for observed wet-snow particles with a diameter ≥ 2.4 mm is 2 m s^{-1} with a standard deviation of 0.8 m s^{-1}. The large standard deviation is likely related to the coexistence of particles of similar physical size with different percentages of melting. These results suggest that different particle sizes are not required for aggregation since wet-snow particles of the same size can have different fall speeds. Given the large standard deviation of fall speeds in wet snow, the collision efficiency for wet snow is likely larger than that of dry snow. For particle sizes between 1 and 10 mm in diameter within mixed precipitation, rain constituted 1% of the particles by volume within the isothermal layer at 0°C and 4% of the particles by volume for the region just below the isothermal layer where air temperatures rise from 0° to 0.5°C. As air temperatures increased above 0.5°C, the relative proportions of rain versus snow particles shift dramatically and raindrops become dominant. The value of 0.5°C for the sharp transition in volume fraction from snow to rain is slightly lower than the range from 1.1° to 1.7°C often used in hydrological models.

1. Introduction

An accurate description of the physical characteristics of coexisting rain and snow near the freezing level is important not only to cloud and regional forecast models (Tao et al. 2003; Stoelinga et al. 2003) but also to the retrieval of precipitation from satellite passive and active microwave measurements (Bauer et al. 1999; Iguchi et al. 2000; Olson et al. 2001). The assumptions about the particle size distributions (PSD) and fall speed relations used in bulk microphysics parameterizations are similar to those required to determine the absorption, scattering, and extinction coefficients within radiative transfer calculations. For the purposes of this paper, we will use the term *wet snow* to refer to

* The National Center for Atmospheric Research is sponsored by the National Science Foundation.

Corresponding author address: Prof. Sandra Yuter, Dept. of Marine, Earth, and Atmospheric Sciences, Box 8208, North Carolina State University, Raleigh, NC 27695.
E-mail: sandra_yuter@ncsu.edu

partially melted aggregates of snowflakes and the term *mixed precipitation* to refer to coexisting rain and wet-snow mixtures excluding graupel or hail.

Melting natural and artificial aggregates of snow crystals have been investigated in the laboratory (Mitra et al. 1990) by dropping individual flakes into the controlled environment of a vertical wind tunnel. However, examination of naturally occurring populations of melting snowflake aggregates has been lacking because of the practical difficulties of distinguishing among the coexisting particle distributions of rain and snow. Dual-polarization radar measurements can distinguish between rain-only and mixed-phase precipitation, but these methods have primarily been applied to the discrimination of hail and graupel from coexisting rain (e.g., Balakrishnan and Zrnić 1990; Brandes et al. 1995). Snow particles with diameter $D > 4$ mm are difficult to observe with aircraft probes because they often break up in probe-associated turbulence. In addition, aircraft-icing safety concerns limit the time aircraft can spend in the melting layer. Ground-based instruments that simultaneously measure particle size and fall speed provide an opportunity to distinguish the characteristics of coexisting rain and snow particles within mixed precipitation.

We utilize observations of precipitation particles with $D > 1$ mm obtained by a Particle Size and Velocity (PARSIVEL) disdrometer, a ground-based instrument that is designed to measure simultaneously the fall speed and size of particles up to 24.5 mm in diameter. We apply a classification method based on particle size and fall speed properties to separate rain particles from snow particles. The separated rain and snow components of the PSD obtained near 0°C are compared with examples of rain-only and dry-snow PSD observations to highlight the unique characteristics of wet snow. The implications of these results for bulk microphysics parameterizations and hydrological modeling are also examined.

2. PARSIVEL disdrometer

a. Description

The PARSIVEL disdrometer (Löffler-Mang and Joss 2000; Löffler-Mang and Blahak 2001) is an optical sensor. A laser diode produces a horizontal sheet of light 30 mm wide, 180 mm long, and 1 mm high. The horizontal sampling area is 5400 mm^2, which is similar to the 5000-mm^2 sampling area of the Joss–Waldvogel disdrometer (Waldvogel 1974). The laser light is received at a photodiode that samples at 50 000 Hz. When particles pass through the light sheet, a portion of the transmitted laser light is blocked and the voltage produced by the photodiode is reduced relative to when no particles are present in the beam. The amplitude of the voltage drop is related to the size of the particle. The duration of the voltage drop is related to the fall speed of the particle. The instrument measures the maximum diameter of the one-dimensional projection of the particle, which is smaller than or equal to the actual maximum diameter. The particle size D and fall speed V for every particle detected over the measuring period are tabulated in an array whose dimensions are the number of size bins by the number of fall speed bins. Because the disdrometer instrument cannot distinguish sizes within a size interval, all particles detected within an interval are assigned the mean size for that interval, yielding a quantization error that can be important, in particular for $D > 10$ mm, where the size interval is ≥ 2 mm. For this study, the raw output arrays, which represent 1-min samples, are accumulated into longer time periods following the method of Joss and Gori (1978). Because the height of the sample volume is a function of fall speed, $n(D, V)_{ij}$, the number concentration of particles per unit size and per unit velocity interval is first computed for each size interval i and fall speed interval j. These values are summed over all of the velocity bins to determine $n(D)_i$ and over all of the size bins to determine $n(V)_j$.

The particle diameter as measured by the PARSIVEL disdrometer is calculated from the maximum reduction of the voltage. A spheroid model[1] derived from Andsager et al. (1999) is used to estimate the size of the particles as a function of voltage reduction. Particles with $D < 1$ mm are assumed to be spherical (axis ratio = 1). For particles with $D > 5$ mm, an axis ratio of 1.3 is used. For particles with D between 1 and 5 mm, the assumed axis ratio varies linearly from 1 to 1.3. Rain particles are assumed to be symmetric in the horizontal plane. Snow particles are often not horizontally symmetric, and thus particle sizes for snow frequently underestimate actual maximum particle diameter (Löffler-Mang and Blahak 2001). The effect of the porosity of snowflake aggregates on the measured size and fall speed has not been investigated. Another important assumption in PARSIVEL data analysis is that it is rare for two particles to be in the light sheet at the same time (Löffler-Mang and Joss 2000). Such a juxtaposition of particles would yield data indicating a large particle falling at either the same speed or slower (if the par-

[1] An earlier version of the PARSIVEL disdrometer used a spherical assumption for all particle sizes (Löffler-Mang and Joss 2000).

ticles were slightly offset in the vertical direction) relative to the constituent particles.

b. Data-quality issues

When only a portion of a particle intersects the beam, the sensor registers a small particle falling faster than other particles observed at that size. The removal of these "margin fallers" (U. Blahak 2003, personal communication) requires assumptions on the natural distribution of fall speeds for small particles. For rain, the natural fall speed distribution is relatively narrow and margin fallers can be distinguished and removed. For snow, the situation is more ambiguous because the size–fall speed distributions for small snow particles and margin fallers overlap. Empirical studies have addressed average fall speeds of ice particles (e.g., Zikmunda 1972; Locatelli and Hobbs 1974), but information on the distribution of snowfall speeds is scarce. To minimize misclassification of margin fallers as small ice particles in mixed precipitation conditions, we have taken the drastic step in our data analysis of removing all small particles with $D < 1$ mm even though the instrument is capable of detecting particles as small as 0.3 mm in diameter. Particles with $D < 1$ mm are important to the calculation of integrated quantities of the particle size distribution such as mixing ratios. However, given a PSD over the full precipitation size range, one can obtain mixing ratios comparable to those obtained in this study by limiting the calculation to size bins with $D > 1$ mm.

Wind and vibration can degrade the performance of the PARSIVEL disdrometer. The manufacturer recommends against deployment of the instrument in windy conditions. The instrument was sheltered from the wind at both locations at which data were collected for this study (section 3).

A possible complication in the measurement of particle size and fall speeds of snow aggregrates is that they may exhibit complex fall trajectories including spinning, spiraling, and shaking (Lew et al. 1986). Because the depth of the light beam is only 1 mm, it is assumed that the influence of complex fall trajectories on the results is negligible.

3. Observations

a. Locations

As part of the Improvement of Microphysical Parameterizations through Observational Verification Experiment (IMPROVE) II (Stoelinga et al. 2003), a suite of instrumentation was deployed at McKenzie Bridge (MKB), Oregon (altitude 494 m MSL) in the foothills of the Oregon Cascade Mountains during December of 2001. The instrument site was in the McKenzie River valley within a flat grassy area adjacent to a rarely used airstrip. In addition to the PARSIVEL disdrometer, other instruments at the site included a vertically pointing S-band Doppler radar (White et al. 2000), a 915-MHz wind profiler (Weber et al. 1993), and surface meteorological instrumentation provided by the National Oceanic and Atmospheric Administration (NOAA) Environmental Technology Laboratory (ETL). The MKB site was well sheltered by surrounding trees. Wind gusts ≥ 4 m s^{-1} occurred for less than 10% of the sampling periods.

To provide a contrast to the rain and mixed precipitation data obtained in Oregon, the PARSIVEL disdrometer was deployed at the Desert Research Institute's Storm Peak Laboratory (SPL) at an altitude of 3200 m MSL (Borys and Wetzel 1997) near Steamboat Springs, Colorado, during February and March of 2003. The objective was to obtain measurements in dry snow. Because the SPL is a mountaintop facility that often experiences high winds, the PARSIVEL disdrometer was placed in an open-topped enclosure near the center of the roof where snowflakes were observed to fall close to vertically. The horizontal light sheet of the disdrometer was about 24 cm from the top of the enclosure. The perturbed airflow over the enclosure would have largest impact on the trajectories of the smallest, lightest particles and least impact on the largest, heaviest particles (Folland 1988).

b. Joint distributions of particle size and fall speed

A rain-only period from 0300 to 0800 UTC 17 December 2001 (Table 1, Fig. 1a) is presented first to familiarize the reader with the data matrix of particle size and fall speed obtained by the PARSIVEL disdrometer. During the 5-h observation period, the air temperature varied from 2.5° to 5.5°C (Fig. 2a) and relative humidity was 98%. The plot shows the quality-controlled matrices of raw particle counts by size and fall speed. Superimposed on the color-coded matrix (Fig. 1) are empirical fall speed relationships for rain r (Berry and Pranger 1974), lump graupel g (Locatelli and Hobbs 1974), and aggregates of unrimed dendrites d (Locatelli and Hobbs 1974). As expected, the distribution of observed fall speeds as a function of diameter clusters closely around the empirical fall speed relation for rain.

A snow event at SPL from 0000 to 1400 UTC 27 February 2003 is used to illustrate the size and fall speed distribution of dry-snow particles. The quality-

TABLE 1. Environmental conditions and PSD statistics for each of the five particle distribution samples shown in Figs. 6 and 8. Note that mixing ratio (q) values are computed for the subset of particles with $D > 1$ mm; q is underestimated relative to estimates that include smaller particle sizes. MKB A, MKB B, and MKB C refer to time periods and air temperature ranges defined in Fig. 2.

	MKB rain	SPL snow	MKB A	MKB B	MKB C
Pressure (hPa)	952	676	957	959	960
Avg temperature (°C)	3.6	−8	1.1	0.3	0
Minutes with precipitation	289	637	195	63	308
Raw particles after quality control	14 503	54 870	12 095	5628	11 575
No. rain	14 457	0	11 545	2282	1373
No. not rain	46	54 870	270	1773	4782
No. ambiguous	—	—	281	1573	5420
q_r (g kg^{-1}) for $D > 1$ mm	0.04	—	0.09	0.05	0.005
q_s (g kg^{-1}) for $D > 1$ mm	—	0.12	—	—	—
q_{ws} (g kg^{-1}) for $D > 1$ mm	—	—	0.004	0.29	0.19

controlled data matrix from SPL is shown in Fig. 1b. The mode of the joint size–fall speed distribution is centered on the empirical fall speed relation for dendrites. The distribution for dry snow tails off as particle diameters approach 10 mm, consistent with the absence of very large snowflake aggregates ($D > 10$ mm). During the observation period, the temperature dropped from −5° to −10°C (Fig. 2b). Relative humidity increased from 92% at 0000 UTC to 100% at 2000 UTC, held steady near 100% until 1000 UTC, and then dropped to 96% at 1400 UTC (not shown). The average wind speed was 4.2 m s^{-1}, with a standard deviation of 1.2 m s^{-1} (not shown).

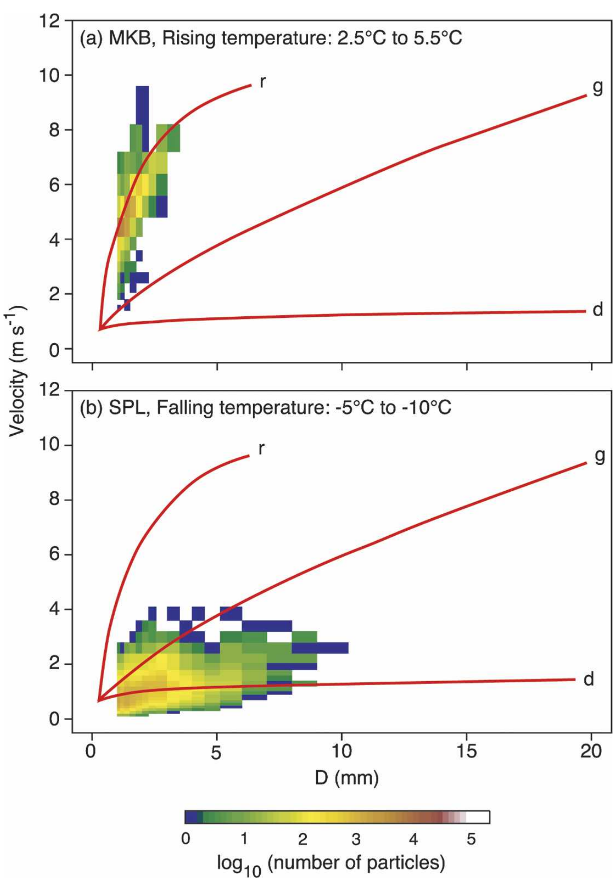

FIG. 1. Accumulated joint size and fall speed distributions of observed particles after quality control is applied (section 2): (a) rain-only event at McKenzie Bridge between 0300 and 0800 UTC 17 Dec 2001 and (b) dry-snow event at Storm Peak from 0000 to 1400 UTC 27 Feb 2003. Empirical fall speed relations from Locatelli and Hobbs (1974) are indicated by red lines (see text): r = rain, g = graupel, and d = dendrite.

The rain-only and dry-snow observations contrast with those in mixed precipitation from MKB on 18–19 December 2001 (Fig. 3). The air temperature dropped from 1.5° to 0°C between 2030 UTC 18 December and 0050 UTC 19 December and then remained at 0°C while precipitation continued to fall for nearly 7 h (Fig. 2c). Quality-controlled matrices of raw particle counts by size and fall speed are shown in Fig. 3 corresponding to three time periods during which the air temperature decreased from 1.5° to 0.5°C (2030–2345 UTC 18 December), decreased from 0.5° to 0°C (2346 UTC 18 December–0049 UTC 19 December), and held steady at 0°C (0050–0600 UTC 19 December). The precipitation was associated with several prefrontal and postfrontal rainbands. The vertically pointing S-band radar data (Fig. 4a) show the decreasing altitude and then disappearance of the higher radar reflectivities (>~33 dBZ) in the radar bright band associated with the melting layer at the top of the rain layer as it drops below the lowest range gate (200 m AGL or 700 m MSL) of the radar at 0000 UTC and then intersects the surface. The hourly averaged profiles of horizontal wind velocity shown in Fig. 4b indicate a near-surface wind shift from southerly to westerly as the front passed at about 1800 UTC. Near-surface winds at the observation site (not shown), measured at 10 m AGL, were light and averaged 0.5 m s^{-1} from 1400 until 0000 UTC when the anemometer froze up. Relative humidity (not shown) remained at 99% throughout the time period. Further

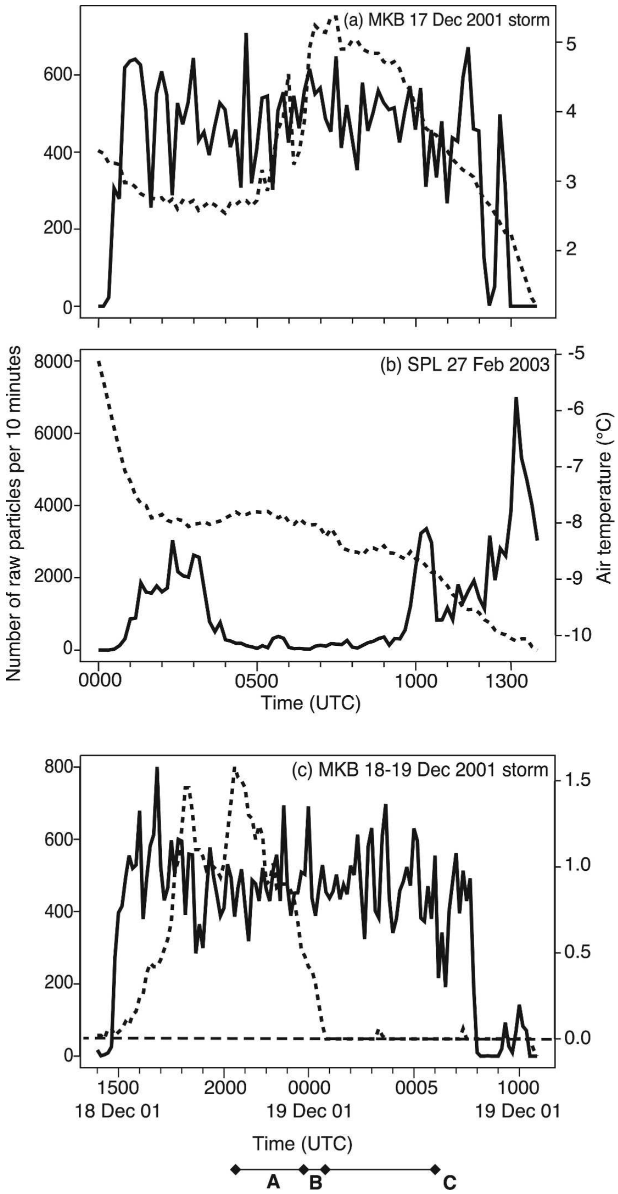

FIG. 2. Time series of the number of particles measured in 10-min intervals by a PARSIVEL disdrometer (solid line) and 10-min-averaged air temperature (dotted line): (a) rain-only event at McKenzie Bridge from 0000 to 1400 UTC 17 Dec 2001, (b) dry-snow event at Storm Peak from 0000 to 1400 UTC 27 Feb 2003, and (c) mixed-precipitation event at McKenzie Bridge from 1400 UTC 18 Dec to 1100 UTC 19 Dec 2001. During the mixed-precipitation event, the time periods A, B, and C correspond to precipitation samples when air temperature decreased from 1.5° to 0.5°C, decreased from 0.5° to 0°C, and held steady at 0°C. In (c), the dashed line shows 0°C temperature.

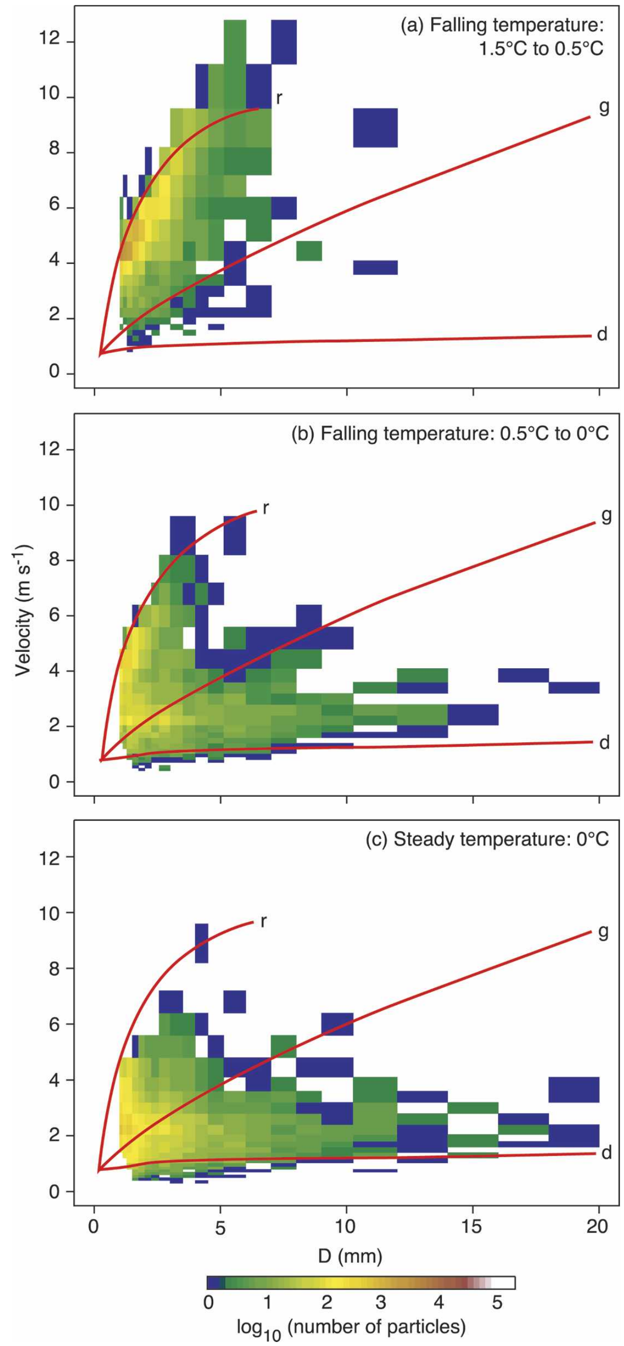

FIG. 3. As in Fig. 1, but for a mixed-precipitation event at McKenzie Bridge: (a) 2030–2345 UTC 18 Dec 2001, (b) 2346 UTC 18 Dec–0049 19 Dec 2001, and (c) 0050–0600 UTC 19 Dec 2001. Times represented in (a)–(c) correspond to intervals A, B, and C defined by temperature in Fig. 2.

details on the environmental setting and observations at McKenzie Bridge and Storm Peak are presented in Table 1.

The distribution of fall speeds for particles of a given size at temperatures from 1.5° to 0.5°C (Fig. 3a) is wider than that for the rain-only time period (Fig. 1a). The PSD distribution from 1.5° to 0.5°C likely includes some particles that are not 100% melted. At tempera-

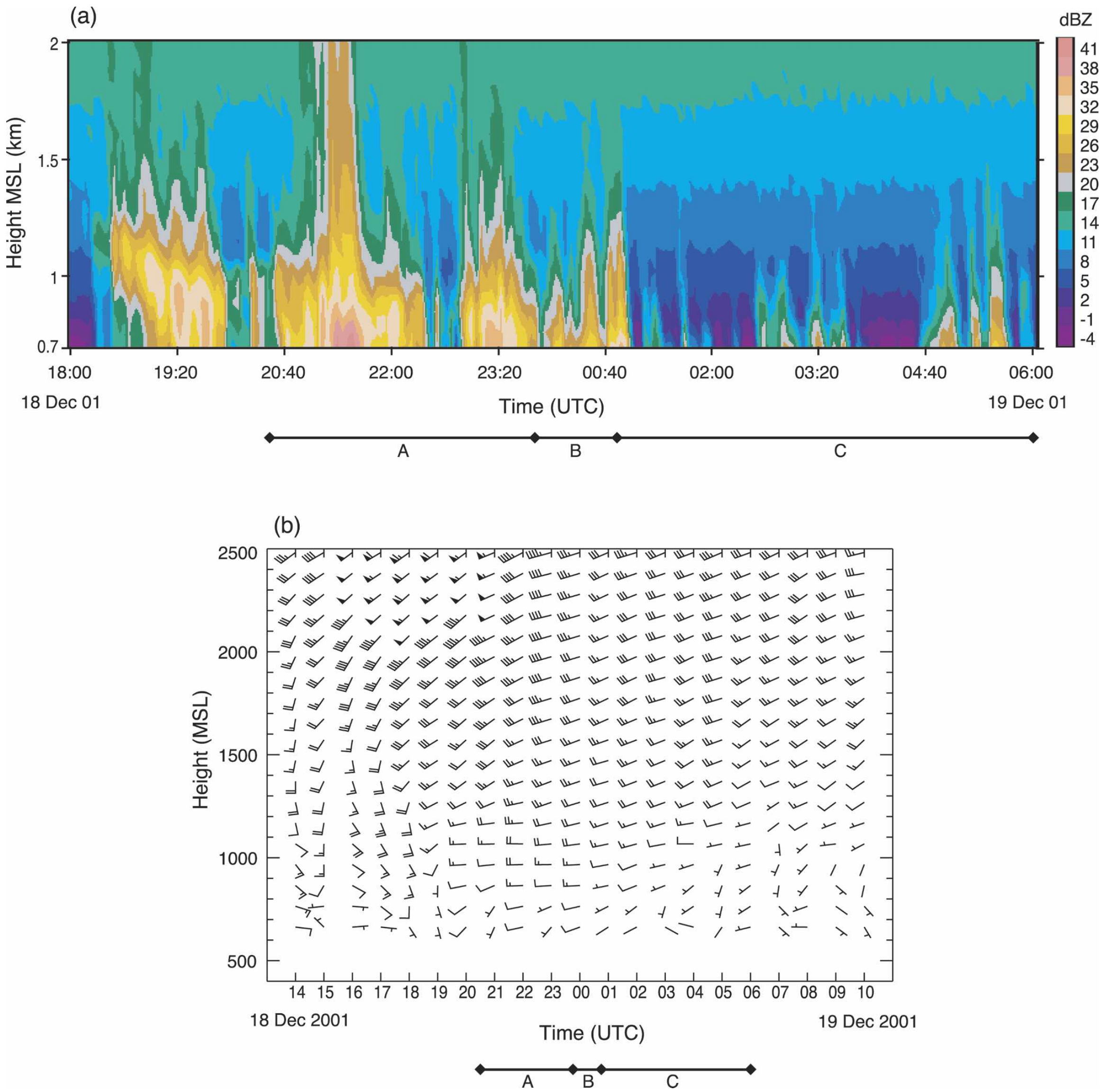

FIG. 4. (a) Time–height plot of 8-s-averaged radar reflectivity measured by the NOAA ETL S-band profiler in 300-ns (low sensitivity) mode at McKenzie Bridge from 1800 UTC 18 Dec to 0600 UTC 19 Dec 2001. The time periods A, B, and C are as shown in Fig. 2. The intensity of the radar bright band varies during this example. Higher-reflectivity portions of the bright band have $Z > 35$ dBZ. Horizontal bands of blue and green correspond to increasing minimum detectable reflectivity with increasing height. The signal was attenuated by snow accumulation on the radar antenna during portions of the time period shown. (b) Time–height plot of hourly NOAA ETL wind profiler data from 14 UTC 18 Dec to 1000 UTC 19 Dec 2001. Wind barbs point into the wind. Wind barb scale: flag = 50 m s^{-1}, full barb = 10 m s^{-1}, and half barb = 5 m s^{-1}.

tures between 0.5° and 0°C, the distribution of particles is bimodal, with distinct populations of rain and snow particles (Fig. 3b). The bimodal distribution of rain and snow particles is not as distinct but is also evident during the period when temperatures held steady at 0°C (Fig. 3c). The maximum size of particles increased as temperatures decreased toward 0°C, in agreement with previous aircraft in situ studies of the melting layer (Stewart et al. 1984; Willis and Heymsfield 1989).

4. Method

a. *Classification of rain, not-rain, and ambiguous subsets*

The particles in the raw data matrix are classified into rain, not-rain, and ambiguous subsets using the masks shown in Fig. 5a. The rain classification is based on the identification of rain particles by their size and fall speed characteristics. The bottom edge of the rain mask

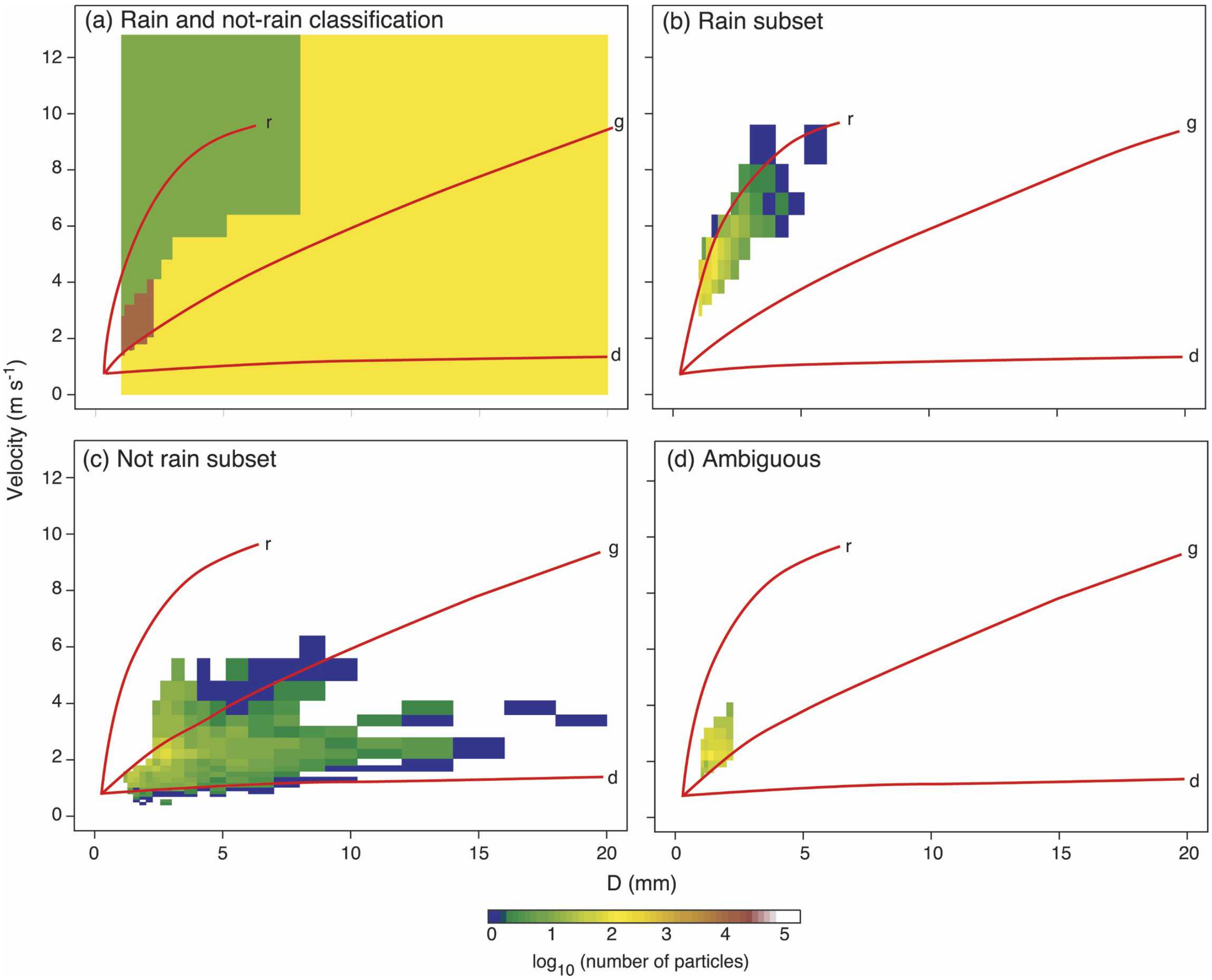

FIG. 5. (a) Mapping of rain (green), not-rain (yellow), and ambiguous (red) classifications on PARSIVEL joint size and fall speed matrix. Application of masks is to data in Fig. 3b. (b) Application of rain classification mask yielding rain subset of particles. (c) Application of not-rain classification mask. (d) Application of ambiguous classification mask.

is defined as the velocity bin that is two bins lower than the velocity bin nearest the empirical fall speed relation for rain. This lower boundary of the rain mask was determined empirically, based on the location of the local minima in the bimodal distributions in Figs. 3b and 3c. In both rain and dry-snow situations, particles were observed with $D < 2.4$ mm and with fall velocities between three and eight bins lower than the empirical fall speed relation for rain. These particles are classified as ambiguous because the combination of size and fall velocity information is insufficient to distinguish snow from rain. All particles not classified as either rain or ambiguous within the joint size–fall speed matrix are classified as not rain. The not-rain category encompasses the empirical fall speed relation for dendrites and also includes all particles with $D > 8$ mm diameter independent of fall speed. The rain, not-rain, and ambiguous subsets of a particular particle distribution are identified (Figs. 5b–d) by applying the relevant mask to the quality-controlled raw distribution (e.g., Fig. 3b). The same classification mask is used for all cases of mixed precipitation. The time-accumulated particle size distributions for the particles classified as ambiguous are shown in Fig. 6. The largest concentrations of ambiguous particles occurred during mixed precipitation at temperatures of 0° and from 0° to 0.5°C (Figs. 6a,b) when small particles with properties between those of ice and rain are most likely to be present.

b. Particle distribution descriptions

Following the notation of Smith (1982), the number concentration of particles with diameters in the interval from D to $D + \Delta D$ is denoted by $N(D)$, where

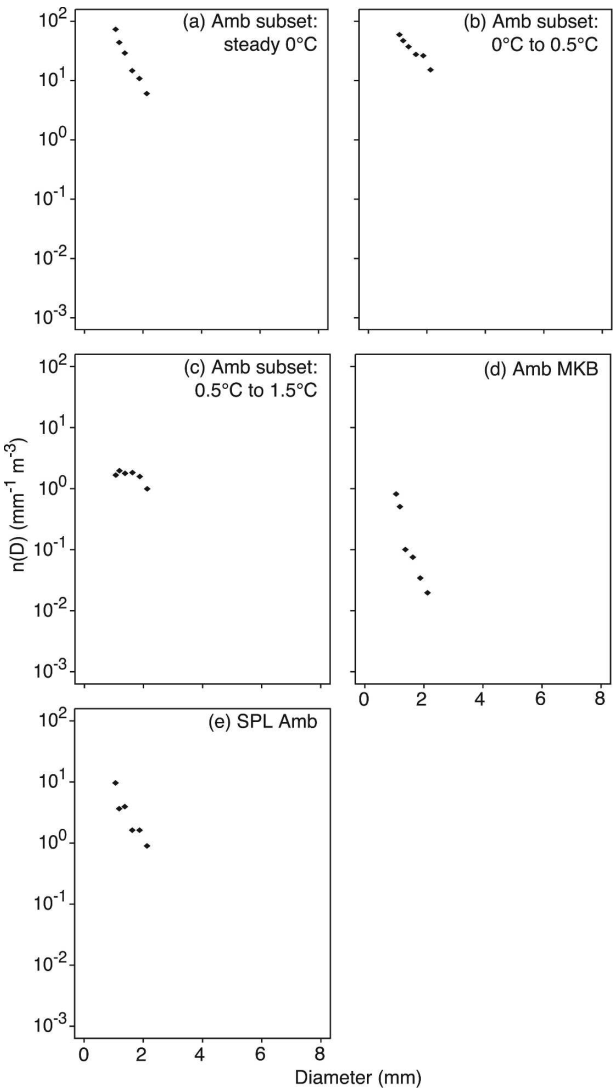

FIG. 6. Time-accumulated particle size distributions for ambiguous subset of classified matrices: (a) McKenzie Bridge 0050–0600 UTC 19 Dec 2001, (b) McKenzie Bridge 2346 UTC 18 Dec–0049 UTC 19 Dec 2001, (c) McKenzie Bridge 2030–2345 UTC 18 Dec 2001, (d) McKenzie Bridge 0300–0800 UTC 17 Dec 2001, and (e) Storm Peak 0000–1400 UTC 27 Feb 2003.

$$N(D) = n(D)\Delta D \tag{1}$$

and $n(D)$ represents the number concentration of particles with diameters in the interval from D to $D + \Delta D$ per unit size interval. In this notation, the exponential size distribution is defined as $n(D) = n_o e^{-\Lambda D}$, where n_o is the intercept at $D = 0$ and Λ is the slope. Smith's notation emphasizes the dependence of $N(D)$, which is the quantity the instrument measures, on the size interval ΔD. The conversion from $N(D)$ to $n(D)$ used in this study relies on the implicit assumption that the average size of particles within each size interval is approximated well by the center value of the size interval. We use the notation $N(V)$, where

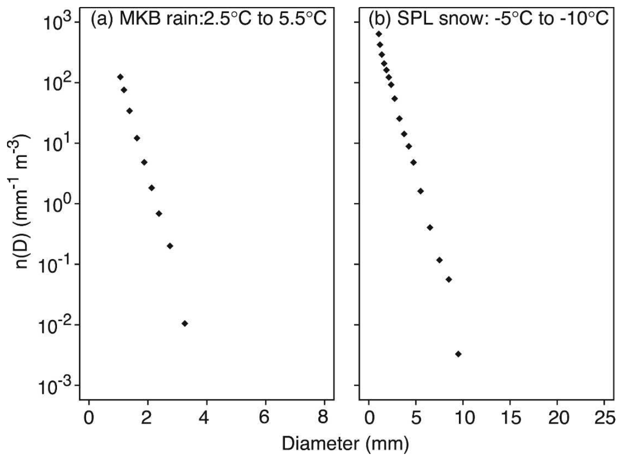

FIG. 7. Accumulated particle size distributions of (a) rain observed at McKenzie Bridge 0300–0800 UTC 17 Dec 2001 and (b) dry snow observed at Storm Peak 0000–1400 UTC 27 Feb 2003. Note that x-axis scale differs between plots.

$$N(V) = n(V)\Delta V, \tag{2}$$

to describe the number concentration of particles with fall speeds in the interval from V to $V + \Delta V$, and $n(V)$ represents the number concentration of particles with fall velocities in the interval from V to $V + \Delta V$ per unit fall velocity interval. We use the notation $\sigma_D(V)$ for the standard deviation of diameter for a given fall speed and $\sigma_V(D)$ for the standard deviation of fall speed for a given diameter.

Mixing ratios (g kg^{-1}) for rain (q_r), dry snow (q_s), and wet snow (q_{ws}) are also calculated as appropriate for the different PSD (Table 1) using

$$q = 10^{-6} \frac{\rho}{\rho_a} \frac{\pi}{6} \sum_i N(D_i) D_i^3, \tag{3}$$

where ρ_a is the density of air at the observed temperature and pressure and ρ is the particle density: 10^6 g m^{-3} for rain, 5×10^4 g m^{-3} for aggregates of dry snow (Heymsfield et al. 2002), and an estimate of 10^5 g m^{-3} for wet snow. Because the analysis for this study only considers particles with $D > 1$ mm, the q values discussed below will differ from those computed when $D < 1$ mm are included.

5. Particle size distribution characteristics

a. Rain and dry snow

The particle size distributions ($D > 1$ mm) shown in Fig. 7 correspond to a time period of rain at MKB (0300–0800 UTC 17 December 2001) and dry snow at SPL (0000–1400 UTC 27 February 2003), respectively.

Similar to findings of previous studies [e.g., rain: Marshall and Palmer (1948); snow: Houze et al. (1979)], these distributions are approximated well by an exponential size distribution. The consistency of the measurements in rain and dry snow with previous results yields confidence in application of the instrument and processing techniques to mixed precipitation.

b. Mixed precipitation

Size distributions computed for the rain and not-rain subsets of particles collected at 0°C are shown in Figs. 8a and 8b. The associated distributions for the ambiguous subset of particles are shown in Fig. 6a. The maximum size of not-rain particles was comparable to those observed in Barthazy's (1998) analysis of in situ observations of stratiform precipitation from a mountainside in Switzerland. Particles with $D > 10$ mm are observed in the not-rain subset. Given their size and associated environmental temperature of 0°C, these large particles are likely partially melted snowflake aggregates (wet snow). The sample volume[2] is $\sim$39 m^3 for an hour of not-rain data, which is equivalent to the sample volume of an aircraft two-dimensional precipitation (2DP) probe along 52 km of flight track that is sampling particles at concentrations of 1 L^{-1} (A. Rangno 2004, personal communication).

During the time period when the temperature decreases from 0.5° to 0°C (Figs. 8c,d), large not-rain particles with $D > 10$ mm are still present, but at lower concentrations than at 0°C. The appearance of large raindrops with $D > 6$ mm (Fig. 8e) coincides with the disappearance of very large snowflake aggregates with $D > 13$ mm (Fig. 8f) within the mixed precipitation as temperature decreases from 1.5° to 0.5°C. The large raindrops with $D > 6$ mm are likely the result of the melting of the larger snowflake aggregates with minimal breakup.

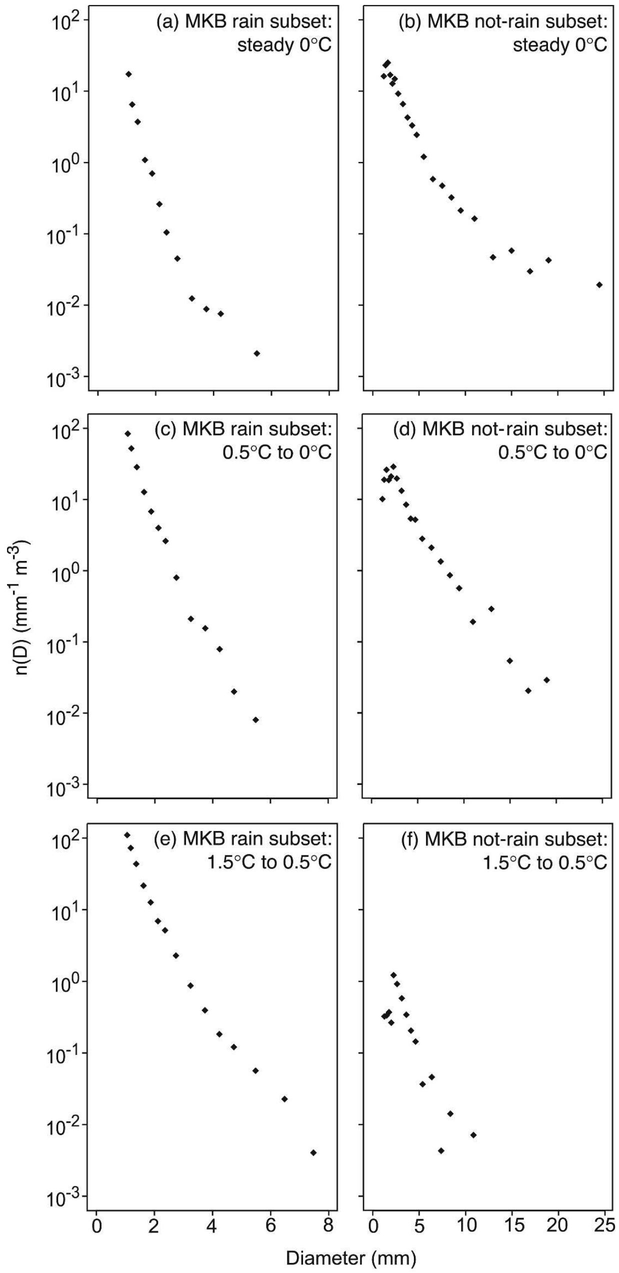

FIG. 8. Time-accumulated particle size distributions for (left) rain and (right) not-rain subsets of classified PARSIVEL matrices from McKenzie Bridge: (a), (b) 0050–0600 UTC 19 Dec 2001; (c), (d) 2346 UTC 18 Dec–0049 UTC 19 Dec 2001; (e), (f) 2030–2345 UTC 18 Dec 2001. Note that *x*-axis scale differs between left and right columns.

6. Fall speed–size relations

The PARSIVEL measurements permit an examination of fall speed versus size relationships for the rain and not-rain subsets of particles. Figure 9 contrasts the fall speed V as a function of D for wet snow, dry snow, and rain. Following the method of Beard (1985), an air density correction is applied as a function of particle diameter to adjust the datasets to conditions at 1000 hPa and 0°C in Figs. 9, 10, and 11. The SPL data (Fig. 9b) indicate the fall speed for dry snow is a monotonically increasing function of particle size. The relationship between fall speed and particle size in the SPL data is similar to that of Locatelli and Hobbs (1974) for unrimed dendrite aggregates [$V(D) = 0.8D^{0.16}$], at least up to particles of 5-mm diameter, the maximum observed particle size in their study. In contrast to dry snow and rain, the fall speeds for wet snow have larger standard

[2] The sample volume is computed assuming an average 2 m s^{-1} fall speed and 180 mm $\times$ 30 mm instrument sampling area.

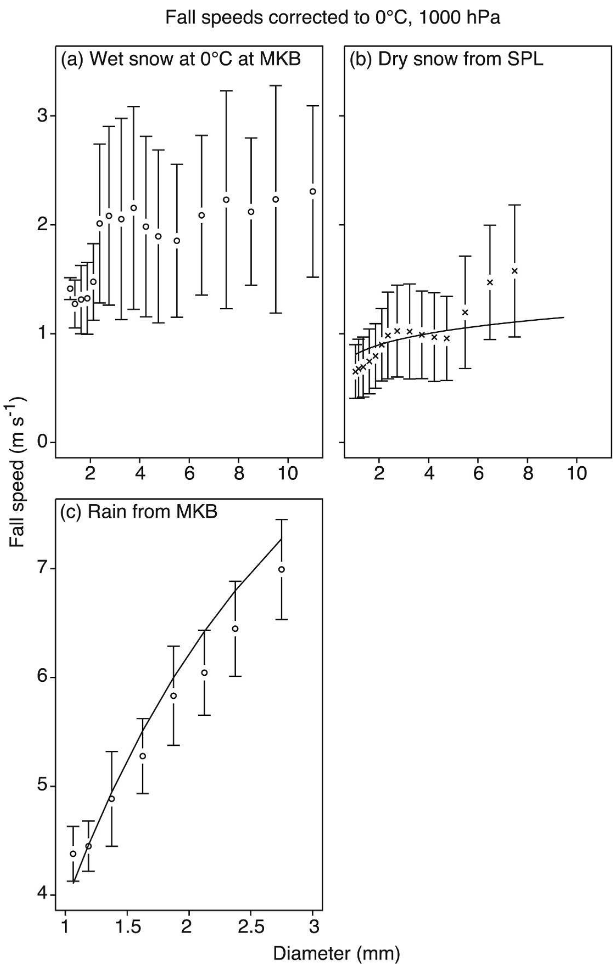

FIG. 9. Mean and standard deviation of particle fall speed as a function of particle diameter D for (a) wet snow at McKenzie Bridge 0050–0600 UTC 19 Dec 2001 while air temperatures held steady at 0°C, (b) dry snow observed at Storm Peak 0000–1400 UTC 27 Feb 2003 while air temperatures dropped from $-5°$ to $-10°$C (overlaid line is empirical fall speed relation for aggregates of unrimed dendrites; Locatelli and Hobbs 1974), and (c) rain observed at McKenzie Bridge 0300–0800 UTC 17 Dec 2001 when temperatures varied between 2.5° and 5.5°C (overlaid line is empirical fall speed for rain; Berry and Pranger 1974). Plot shows only data bins for raw particle counts ≥20 (see the appendix). The y axis is at same relative scale (3.5 m s^{-1}) for all three plots. Fall speeds are adjusted to air density at 0°C and 1000 hPa following the method of Beard (1985).

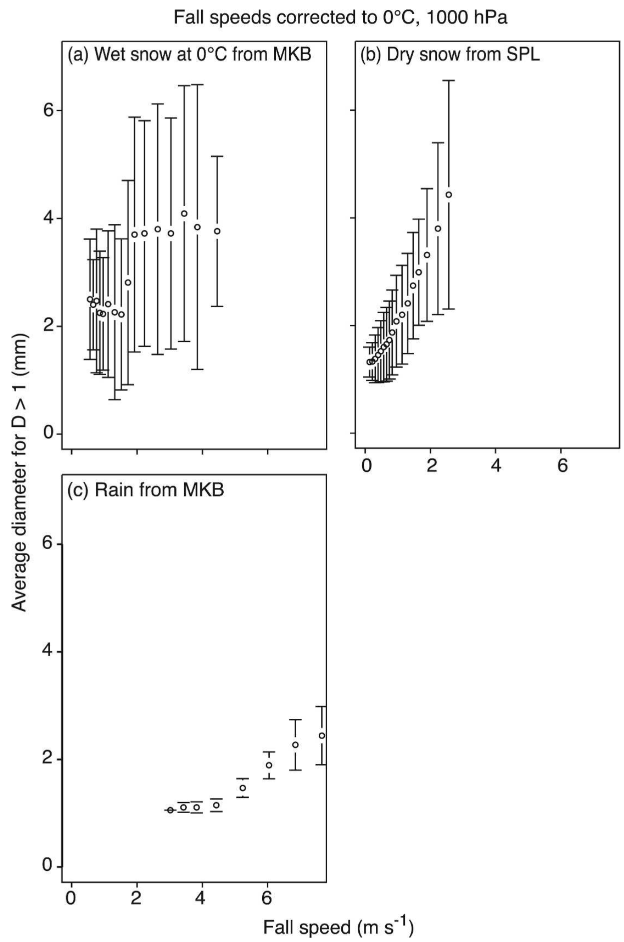

FIG. 10. Datasets as in Fig. 9. Mean and standard deviation of particle size (for subset of particles with $D > 1$ mm) as a function of fall speed. Plot shows only data bins for raw particle counts ≥20 (see the appendix).

deviations and are poorly correlated to particle size for $D \geq 2.4$ mm (Fig. 9a). The average fall speed of wet snow with D between 2.4 and 11 mm is 2 m s^{-1} (Fig. 9a). The standard deviations in fall velocity for a given D are also larger [mean $\sigma_V(D) = 0.8$ m s^{-1}; maximum $\sigma_V(D) = 1$ m s^{-1}] than those for dry snow [mean $\sigma_V(D) = 0.4$ m s^{-1}; maximum $\sigma_V(D) = 0.6$ m s^{-1}] or rain [mean $\sigma_V(D) = 0.4$ m s^{-1}; maximum $\sigma_V(D) = 0.5$ m s^{-1}]. Mitra et al. (1990) found that the fall velocity of melting snowflake aggregates increased nonlinearly with an increasing percentage of mass melted and that this relation was nearly independent of the initial size of the snowflake. We hypothesize that variations in the percentage of mass melted among sampled particles of the same diameter could explain the large standard deviations in the measured wet-snow fall speeds.

The fall speed–size data in Fig. 9 are presented in terms of average diameter as a function of fall speed by summing along velocity bins rather than diameter bins. Figure 10 shows the variability in average D, where $D > 1$ mm, for a given fall speed interval for wet and dry snow and rain. For rain, $\sigma_D = 0.09$ mm at $V = 3.4$ m s^{-1} and $\sigma_D = 0.17$ mm at $V = 5.2$ m s^{-1}. For wet snow, the average size of particles falling at $V > 1$ m s^{-1} first decreases and then increases. The standard deviations $\sigma_D(V)$ of the diameter for a given fall speed are large: $\sigma_D = 2.2$ mm at $V = 1.9$ m s^{-1} and $\sigma_D = 2.4$ mm

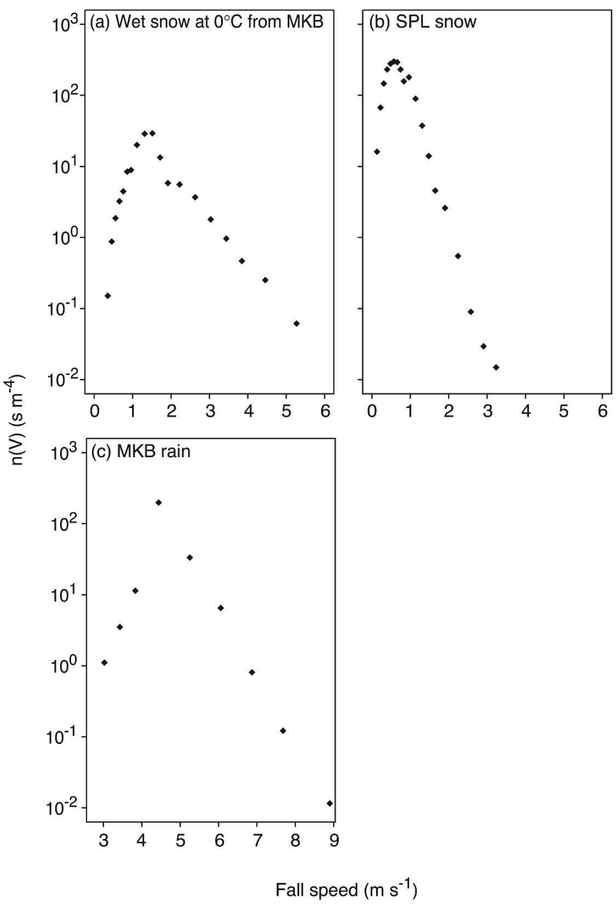

FIG. 11. Accumulated fall velocity distributions $n(V)$ for datasets as in Fig. 9. Note that x-axis scale differs among plots but the dynamic range is 6 m s^{-1} for all three plots.

at $V = 3.4$ m s^{-1}. The $D(V)$ relation for dry snow reveals a trend of increasing variability in D with increasing V. For dry snow, $\sigma_D = 0.99$ mm at $V = 1.9$ m s^{-1} and $\sigma_D = 2.1$ mm at $V = 3.4$ m s^{-1}. Zikmunda (1972) attributed scatter in fall velocity of dry-snow aggregates to variations in aggregate shape. Figure 11 shows the observed $n(V)$ for the wet-snow, dry-snow, and rain datasets. This figure illustrates the skewed distribution of fall speeds around the modal fall speed of each PSD: 1.9 m s^{-1} for wet snow, 0.54 m s^{-1} for dry snow, and 4.3 m s^{-1} for rain.

Ralph et al. (1995) used the variance of Doppler velocity to distinguish among snow, melting layer, and rain using vertically pointing 404-MHz profiler data. The current study provides in situ verification of this result and clarifies that at least part of the variance difference is related to the differing variance of fall speeds between wet and dry snow.

Turbulence is often observed near the melting layer (Willis and Heymsfield 1989; Steiner et al. 2003). However, the influence of turbulence on our fall speed measurements at MKB is likely limited. The measurement height of the PARSIVEL is 1 m above the surface. Surface friction will act to dampen any preexisting turbulence. The recorded horizontal wind speeds at 10 m AGL were low, averaging 0.5 m s^{-1}. Given the higher wind speeds observed at SPL, the influence of turbulent eddies on the size–fall speed relation is likely to be greater at SPL than MKB. In addition, one would expect turbulence to have a larger impact on the smaller, lighter particles, which is the opposite of what is observed.

7. Implications

a. *Microphysical processes*

Aggregation is an important component of the microphysical processes as temperatures increase toward 0°C. Bulk microphysics parameterizations, such as Lin et al. (1983), account for transformations among water substance categories but do not usually account for processes like aggregation that transform the particle size distribution within a single water substance category. The large standard deviation of wet-snow fall speeds observed at MKB indicates that different particle sizes are not required for aggregation since wet-snow particles of the same size can have different fall speeds. Hence, the collision efficiency for wet snow is likely larger than that of dry snow, which has a smaller standard deviation of fall speeds, and average fall speeds that monotonically increase with particle size. In the MKB observations, aggregation yielded snow distributions that contained very large snowflake aggregates ($D > 10$ mm).

The weak correlation between wet-snow particle size and fall speed is also of potential importance to bulk microphysical parameterizations because it calls into question the use of a monotonic fall speed relation for wet snow. An alternative method to parameterize the size–fall speed relationship of wet-snow particles with $D > 2$ mm would be to use a probability distribution of fall speeds. For conditions similar to those sampled, a distribution with mean $V(D) = 2$ m s^{-1} and standard deviation of $\sigma_V(D) = 0.8$ m s^{-1} would better approximate observed fall speeds than would a monotonically increasing relationship. The ensemble behavior of such particles could be modeled to refine the aggregation rates for wet snow.

In the MKB data, the reduction in the number of the very large snowflake aggregates as air temperatures increased coincided with the appearance of rain particles larger than 6 mm in diameter. These results suggest that the breakup of large snowflake aggregates in the

TABLE 2. Relative proportions of rain subset of particles during mixed precipitation at McKenzie Bridge. Note that statistics are calculated for subset of particles with 1 mm $\leq D \leq$ 10 mm.

Air temperature	Percent of rain particles of total concentration (No. m^{-3})	Percent rain volume of total volume	Avg rain rate (mm h^{-1})	Rain D_{max} (mm)
0°C	5%	1%	0.09	5.5
0.5°–0°C	23%	4%	1.0	5.5
1.5°–0.5°C	93%	74%	2.3	7.5

sampled stratiformlike conditions is minimal. Lack of evidence for the breakup of snowflake aggregates is consistent with Ohtake's (1969) study of the size distributions of melted snow falling at mountainside stations in Japan and Alaska. In their observations of very large snowflakes up to 5 cm in diameter in a winter storm off the coast of Newfoundland, Canada, Lawson et al. (1998) also found evidence of rapid aggregation near the 0°C region without appreciable particle breakup. Drummond et al. (1996) estimated the occurrence of aggregration versus breakup within the melting layer using vertically pointing 915-MHz radar reflectivity and Doppler vertical velocity measurements above and below the melting layer. They found that aggregation was dominant most of the time. Breakup was associated with higher reflectivities and heavier precipitation rates than those sampled in this study.

b. Hydrological modeling

Hydrological models categorize precipitation by surface air temperature. The temperature threshold between rain and snow is traditionally defined as 1.1°–1.7°C (34°–35°F; U.S. Army Corps of Engineers 1956). Precipitation falling through surface air temperatures higher than this threshold is categorized as rain, and precipitation falling at lower temperatures is categorized as snow. This categorization by temperature is consistent with data presented in Table 2, but a sharp transition from all rain to all snow oversimplifies the situation between 1.1° and 0°C, where rain and snow coexist. The MKB data indicate that a dramatic shift occurs in the relative proportions of rain and snow particles near 0.5°C. Snow dominates over rain in terms of number and volume fraction for temperatures of 0°–0.5°C. At temperatures higher than 0.5°C, raindrops become the dominant particle type. These results indicate that the majority of large snow particles are fully melted by 0.5°C at MKB, although a small fraction of larger flakes persists to higher temperatures. Willis and Heymsfield (1989) found large aggregates at air temperatures of 5°C.

The coexisting rain rates associated with snow at and near 0°C represent potential refinements to parameterizations within hydrological models for mountain flood-forecasting applications. The light rainfall (Table 2) that coexists with snow at 0°C and between 0.5° and 0°C would be difficult to observe with conventional tipping-bucket rain gauges. Over several hours, the accumulation of the light rainfall, even the underestimated rain rates excluding $D < 1$ mm in Table 2, may potentially be significant to hydrological forecasting. Flooding in the mountains of the western United States is sometimes associated with rain falling on snow (Marks et al. 1998; Taylor and Hatton 1999).

8. Conclusions

The PARSIVEL disdrometer (Löffler-Mang and Joss 2000) can simultaneously measure particle fall speed and particle size up to 24.5 mm in diameter. In combination with empirical relations for fall speed, the PARSIVEL data can be subdivided into rain, not-rain, and ambiguous classes and the characteristics of each subset analyzed separately (section 4).

On 18–19 December 2001, a mixed-precipitation event occurred with a combination of rain and wet snow as the temperature at McKenzie Bridge dropped from 1.5° to 0°C over 4.3 h and then remained at 0°C for 7.2 h during a precipitation event (Fig. 2). The stratiform nature of the precipitation at McKenzie Bridge is evident from the layered structure of the radar data (Fig. 4). We contrast these data with those obtained during a 5-h rain event at McKenzie Bridge for which the average air temperature was 3.6°C and a 14-h dry-snow event at Storm Peak for which the temperatures were between −5° and −10°C (Fig. 2). Particle classification using size and fall speed (Fig. 5) applied to surface in situ measurements obtained at McKenzie Bridge and Storm Peak illustrates some key differences in joint fall speed–size characteristics within rain, dry snow, and wet snow.

Within mixed precipitation, the bimodal distribution of the joint fall speed–size characteristics at air temperatures from 0.5° to 0°C (Fig. 3b) suggests that, once melting has progressed sufficiently, wet-snow particles make a quick transition to rain and do not linger in a state the characteristics of which are intermediate between those of wet snow and rain. The disappearance of very large snowflake aggregates ($D > 13$ mm) as air temperatures increase above 0.5°C coincides with the appearance of large rain drops with $D > 6$ mm (Fig. 8), suggesting that breakup of large aggregates is minimal in the conditions sampled. For particles with $D > 2.4$ mm, the average fall speed has a much weaker correlation with size in comparison with dry snow or rain (Fig. 9). The standard deviation of fall speed for wet snow is between 120% and 230% of the standard deviation for similarly sized particles of dry snow. The fall velocity of wet-snow particles with $D \geq 2.4$ mm obtained at 0°C is 2 ± 0.8 m s^{-1}. The large standard deviation is likely related to the coexistence of particles of similar physical size with different degrees of melting. Given the large standard deviation of fall speeds, different particle sizes are not required for aggregation and aggregation rates are likely higher for wet snow as compared with dry snow.

As expected, raindrops constituted a small fraction of the larger precipitation particles at 0°C. For particle sizes between 1 and 10 mm in diameter within mixed precipitation, rain constituted 1% of the particles by volume within the isothermal layer at 0°C and 4% of the particles by volume for the region just below the isothermal layer where air temperatures rise from 0° to 0.5°C (Table 2). The associated light rainfall coexisting with snow is not currently included in most hydrological models. Persistent light rainfall for several hours could potentially yield accumulations relevant to hydrological forecasting. Near 0.5°C, the relative proportions of rain versus snow particles shift dramatically and raindrops become dominant. The majority of snow particles are fully melted by the time they descend to air temperatures of 0.5°C. These observational results differ slightly from the temperature threshold of 1.1°–1.7°C differentiating rain and snow that is commonly used in hydrological models (U.S. Army Corps of Engineers 1956).

Future measurements are needed to extend the in situ dataset, in particular for large particles within mixed precipitation and under a wider range of conditions. Complementary instrumentation is often deployed together because it is difficult to design a single instrument to measure all of the desired quantities of the particle size distribution. Our future deployments of the PARSIVEL disdrometer will ideally include instrumentation to distinguish among particle types at $D < 1$ mm and to measure the equivalent liquid water content of falling snow. Collocated radar and passive microwave sensors would provide context for the in situ measurements and would help to define the natural variability of these remote sensing measurements in relation to the variability of the particle size distributions. The winter precipitation climatological conditions and mountain topography of Oregon and Washington are well suited to observing the melting layer with surface-based instruments.

TABLE A1. Quality-controlled raw particle counts (No. m^{-3}) shown in Fig. 9 by size class for not-rain particles from MKB 0°C and SPL datasets and for rain particles from MKB rain dataset. Size classes 1 and 2 are outside of the instrument range and are not used. Particles in size classes smaller than 1 mm are removed in the quality control (section 2).

i	Mean size (mm)	Width (mm)	MKB 0°C	SPL	MKB rain
3	0.312	0.125	—	—	—
4	0.437	0.125	—	—	—
5	0.562	0.125	—	—	—
6	0.687	0.125	—	—	—
7	0.812	0.125	—	—	—
8	0.937	0.125	—	—	—
9	1.062	0.125	—	9351	5536
10	1.187	0.125	238	6336	3411
11	1.375	0.250	589	8949	3332
12	1.625	0.250	623	6722	1269
13	1.875	0.250	420	5667	553
14	2.125	0.250	351	4760	215
15	2.375	0.250	510	3814	85
16	2.750	0.500	630	4588	53
17	3.250	0.500	421	2097	3
18	3.750	0.500	285	1130	0
19	4.250	0.500	198	680	0
20	4.750	0.500	139	357	0
21	5.500	1.000	134	289	0
22	6.500	1.000	71	89	0
23	7.500	1.000	54	26	0
24	8.500	1.000	37	14	0
25	9.500	1.000	23	1	0
26	11.000	2.000	33	0	0
27	13.000	2.000	8	0	0
28	15.000	2.000	8	0	0
29	17.000	2.000	4	0	0
30	19.000	2.000	5	0	0
31	21.500	3.000	0	0	0
32	24.000	3.000	1	0	0

Acknowledgments. Greatly appreciated are the help and advice of Eduard Beck, Ulrich Blahak, Randy Borys, Brian Colle, Kim Comstock, Daniel Gottas, Brad Smull, Dave Spencer, Ed Mauer, and Allen White. Candace Gudmundson edited the manuscript, and Kay Dewar and Beth Tully drafted the figures. Isztar Zawadski provided constructive criticism on the material. The PARSIVEL instrument loan for IMPROVE II was through the courtesy of the University of Karlsruhe and PMTech, Inc. The work of the first author was supported by NSF Grants ATM-

TABLE A2. Quality-controlled raw particle counts (No. m^{-3}) by velocity class shown in Fig. 10 for not-rain particles from MKB 0°C and SPL datasets and for rain particles from MKB rain dataset.

i	Mean velocity (m s^{-1})	Width (m s^{-1})	MKB 0°C	SPL	MKB rain
1	0.05	0.1	0	0	0
2	0.15	0.1	0	68	0
3	0.25	0.1	0	473	0
4	0.35	0.1	2	1473	0
5	0.45	0.1	9	3118	0
6	0.55	0.1	25	4798	0
7	0.65	0.1	52	6299	0
8	0.75	0.1	80	7227	0
9	0.85	0.1	170	6718	0
10	0.95	0.1	203	5532	0
11	1.10	0.2	538	7987	0
12	1.30	0.2	748	4905	0
13	1.50	0.2	1100	2899	0
14	1.70	0.2	1207	1674	0
15	1.90	0.2	1279	840	0
16	2.20	0.4	2205	659	0
17	2.60	0.4	1537	156	0
18	3.00	0.4	693	31	34
19	3.40	0.4	241	9	127
20	3.80	0.4	74	4	462
21	4.40	0.8	46	0	9630
22	5.20	0.8	15	0	3302
23	6.00	0.8	1	0	753
24	6.80	0.8	0	0	121
25	7.60	0.8	0	0	26
26	8.80	1.6	0	0	2
27	10.40	1.6	0	0	0
28	12.00	1.6	0	0	0
29	13.60	1.6	0	0	0
30	15.20	1.6	0	0	0
31	17.60	3.2	0	0	0
32	20.80	3.2	0	0	0

0121963 and 0630529 and NASA TRMM Grants NAG5-9750 and NNG04GF33A. The work of the second author was supported by NASA TRMM Grants NAG5-9716 and NNG04GJ15G.

APPENDIX

Raw Counts by Fall Speed and *D*

Quality-controlled raw particle counts (number per cubic meter) are given in Table A1 by size class (used in Fig. 9) and in Table A2 by velocity class (used in Fig. 10).

REFERENCES

Andsager, K., K. V. Beard, and N. F. Laird, 1999: Laboratory measurements of the axis ratios for large raindrops. *J. Atmos. Sci.,* **56,** 2673–2683.

Balakrishnan, N., and D. S. Zrnić, 1990: Estimation of rain and hail rates in mixed-phase precipitation. *J. Atmos. Sci.,* **47,** 565–583.

Barthazy, E., 1998: Microphysical properties of the melting layer. Ph.D. thesis, ETH, Zürich, 128 pp.

Bauer, P., J. P. V. Poiares Baptisa, and M. De Iulis, 1999: The effect of the melting layer on the microwave emission of clouds over the ocean. *J. Atmos. Sci.,* **56,** 852–867.

Beard, K. V., 1985: Simple altitude adjustments to raindrop velocities for Doppler radar analysis. *J. Atmos. Oceanic Technol.,* **2,** 468–471.

Berry, E. X., and M. R. Pranger, 1974: Equations for calculating the terminal velocities of water drops. *J. Appl. Meteor.,* **13,** 108–113.

Borys, R. D., and M. A. Wetzel, 1997: Storm Peak Laboratory: A research, teaching, and service facility for the atmospheric sciences. *Bull. Amer. Meteor. Soc.,* **78,** 2115–2123.

Brandes, E. A., V. Vivekanandan, J. D. Tuttle, and C. J. Kessinger, 1995: A study of thunderstorm microphysics with multiparameter radar and aircraft observations. *Mon. Wea. Rev.,* **123,** 3129–3143.

Drummond, F. J., R. R. Rogers, S. A. Cohn, W. L. Ecklund, D. A. Carter, and J. S. Wilson, 1996: A new look at the melting layer. *J. Atmos. Sci.,* **53,** 759–769.

Folland, C. K., 1988: Numerical models of the raingauge exposure problem, field experiments and an improved collector design. *Quart. J. Roy. Meteor. Soc.,* **114,** 1485–1516.

Heymsfield, A. J., S. Lewis, A. Bansemer, J. Iaquinta, L. M. Miloshevich, M. Kajikawa, C. Twothy, and M. Poellot, 2002: A general approach for deriving the properties of cirrus and stratiform ice properties. *J. Atmos. Sci.,* **59,** 3–29.

Houze, R. A., Jr., P. V. Hobbs, P. H. Herzegh, and D. B. Parsons, 1979: Size distributions of precipitation particles in frontal clouds. *J. Atmos. Sci.,* **36,** 156–162.

Iguchi, T., T. Kozu, R. Meneghini, J. Awaka, and K. Okamoto, 2000: Rain-profiling algorithm for TRMM precipitation radar. *J. Appl. Meteor.,* **39,** 2038–2052.

Joss, J., and E. G. Gori, 1978: Shapes of raindrop size distributions. *J. Appl. Meteor.,* **17,** 1054–1061.

Lawson, R. P., R. E. Stewart, and L. J. Angus, 1998: Observations and numerical simulations of the origin and development of very large snowflakes. *J. Atmos. Sci.,* **55,** 3209–3229.

Lew, J. K., D. C. Montague, H. R. Pruppacher, and R. M. Rasmussen, 1986: A wind tunnel investigation of the rimming of snowflakes. Part II: Natural and synthetic aggregates. *J. Atmos. Sci.,* **43,** 2410–2417.

Lin, Y.-L., R. D. Farley, and H. D. Orville, 1983: Bulk parameterization of the snow field in a cloud model. *J. Climate Appl. Meteor.,* **22,** 1065–1092.

Locatelli, J. D., and P. V. Hobbs, 1974: Fall speeds and masses of solid precipitation particles. *J. Geophys. Res.,* **79,** 2185–2197.

Löffler-Mang, M., and J. Joss, 2000: An optical disdrometer for measuring size and velocity of hydrometeors. *J. Atmos. Oceanic Technol.,* **17,** 130–139.

——, and U. Blahak, 2001: Estimation of the equivalent radar reflectivity factor from measured snow size spectra. *J. Appl. Meteor.,* **40,** 843–849.

Marks, D., J. Kimball, D. Tingey, and T. Link, 1998: The sensitivity of snowmelt processes to climate conditions and forest cover during rain-on-snow: A case study of the 1996 Pacific Northwest flood. *Hydrol. Processes,* **12,** 1569–1587.

Marshall, J. S., and W. McK. Palmer, 1948: The distribution of raindrops with size. *J. Meteor.,* **5,** 165–166.

Mitra, S. K., O. Vohl, M. Ahr, and H. R. Pruppacher, 1990: A wind tunnel and theoretical study of the melting behavior of atmospheric ice particles. IV: Experiment and theory for snow flakes. *J. Atmos. Sci.,* **47,** 584–591.

Ohtake, T., 1969: Observations of size distributions of hydrometeors through the melting layer. *J. Atmos. Sci.,* **26,** 545–557.

Olson, W. S., P. Bauer, N. F. Viltard, D. E. Johnson, W.-K. Tao, R. Meneghini, and L. Liao, 2001: A melting-layer model for passive/active microwave remote sensing applications. Part I: Model formulation and comparison with observations. *J. Appl. Meteor.,* **40,** 1145–1163.

Ralph, F. M., P. J. Nieman, D. W. van de Kamp, and D. C. Law, 1995: Using spectral moment data from NOAA's 404-MHz radar wind profilers to observe precipitation. *Bull. Amer. Meteor. Soc.,* **76,** 1717–1739.

Smith, P. L., 1982: On the graphical presentation of raindrop size data. *Atmos.–Ocean,* **20,** 4–16.

Steiner, M., O. Bousquet, R. A. Houze Jr., B. F. Smull, and M. Mancini, 2003: Airflow within major Alpine river valleys under heavy rainfall. *Quart. J. Roy. Meteor. Soc.,* **129,** 411–431.

Stewart, R. E., J. D. Marwitz, J. C. Pace, and R. E. Carbone, 1984: Characteristics through the melting layer of stratiform clouds. *J. Atmos. Sci.,* **41,** 3227–3237.

Stoelinga, M. T., and Coauthors, 2003: Improvement of Microphysical Parameterizations through Observational Verification Experiments (IMPROVE). *Bull. Amer. Meteor. Soc.,* **84,** 1807–1826.

Tao, W.-K., and Coauthors, 2003: Microphysics, radiation and surface processes in the Goddard Cumulus Ensemble (GCE) model. *Meteor. Atmos. Phys.,* **82,** 97–137.

Taylor, G. H., and R. R. Hatton, 1999: *The Oregon Weather Book: A State of Extremes*. Oregon State University Press, 242 pp.

U.S. Army Corps of Engineers, 1956: Summary report of the snow investigations—Snow hydrology. North Pacific Division Rep., 437 pp. [Available online at http://www.crrel.usace.army.mil/icejams/Reports/1956%20Snow%Hydrology%20Report.htm.]

Waldvogel, A., 1974: The N_o jump in raindrop spectra. *J. Atmos. Sci.,* **31,** 1067–1078.

Weber, B. L., D. B. Wuertz, D. C. Welsh, and R. McPeek, 1993: Quality controls for profiler measurements of winds and RASS temperatures. *J. Atmos. Oceanic Technol.,* **10,** 452–464.

White, A. B., J. R. Jordan, B. E. Martner, F. M. Ralph, and B. W. Bartram, 2000: Extending the dynamic range of an S-band radar for cloud and precipitation studies. *J. Atmos. Oceanic Technol.,* **17,** 1226–1234.

Willis, P. T., and A. J. Heymsfield, 1989: Structure of the melting layer in mesoscale convective system stratiform precipitation. *J. Atmos. Sci.,* **46,** 2008–2025.

Zikmunda, J., 1972: Fall velocities of spatial crystals and aggregates. *J. Atmos. Sci.,* **29,** 1511–1515.